On Measuring Sensible-Heat Flux With Airborne Thermometers

William Cooper[1], Adriana Bailey[1], and Joshua Carnes[1]

[1]Earth Observing Laboratory, National Center for Atmospheric Research 80307-3000 Boulder, CO, United States

Correspondence: William Cooper (cooperw@ucar.edu)

Abstract. Most measurements of temperature from research aircraft rely on sensors that have inadequate response for demanding applications, including especially measuring the flux density of sensible heat. In order to improve that measurement, this paper uses in-flight measurements to determine the frequency-domain transfer function that characterizes the time response of standard airborne temperature sensors. Those thermometers sense the "recovery temperature" produced when air is compressed on approach to the sensor. The change in temperature produced by that compression, termed "dynamic heating" in this paper, fluctuates as the airspeed changes, and those changes in airspeed are measured so the expected fluctuations in recovery temperature are known. In this study, flight segments were used where such turbulent fluctuations were the dominant cause of fluctuations in the recovery temperature so that the sensor response could be used to find the transfer function. Examples and a simulation illustrate that, without correction, measurements of sensible-heat flux with a standard sensor can be more than 30% too low, while the proposed correction procedure removes this error. An additional result of the study is the identification of a source of error, prevalent in most archived temperature measurements from research aircraft, that results when conventional treatments of dynamic heating do not take into account the time response of the sensor.

1 Introduction

Research aircraft routinely measure air temperature, but standard sensors do not respond fast enough to meet many scientific needs. In particular, measurements of the flux of sensible heat require faster response than is typically available, as do measurements of near-discontinuous changes such as those at the top of boundary layers or at cloud boundaries. The measurement of sensible-heat flux requires, for the standard eddy-correlation measurement, that temperature be measured with sufficient response to resolve the spectrum of contributions to the flux.

The eddy-correlation measurement of the flux density of sensible heat (F_s) is evaluated from the mean value of this expression (c.f., e.g., Hartmann (2016)):

$$F_s = \rho_a \, C_p \, \langle w' T' \rangle \tag{1}$$

where ρ_a is the density of air, C_p the specific heat of air at constant pressure, w the vertical wind, and T the temperature. Primes in this equation denote fluctuations from the mean and angle brackets denote an ensemble average. Additional information regarding measuring fluxes by eddy correlation is contained in, e.g., Lenschow (1995).

The measurement thus depends on having a temperature sensor that can respond to the range of fluctuations making significant contributions to the flux. Friehe and Khelif (1992) suggested that 4–5 Hz is "just adequate" (for flight at around $125\,\mathrm{m\,s^{-1}}$)

and that 25 Hz would be desirable. If the response of the temperature sensor is incomplete or shifted in phase at a particular frequency, an error will be introduced into the measurement of sensible-heat flux. To avoid significant errors, it therefore is essential to characterize the time response of the temperature sensor used and, where necessary, to apply corrections to compensate for that response.

2 Determining the Transfer Function

The time response of an airborne thermometer can be characterized by a frequency-domain transfer function that relates the measurement (the sensor output) to the measurand (the temperature). This section presents the transfer functions for some standard sensors. Two coupled differential equations with three parameters are proposed as the basis for this characterization, but the frequency-domain transfer function is determined independent of those equations. When the equations predict a transfer function matching the observations, they provide a useful generalization. Furthermore, the parameters in those equations can be constrained with low uncertainty by fitting to the observed transfer functions. The transfer functions then are used in the sections that follow to access how measurements of temperature are affected.

Because airborne thermometers respond to the temperature of the air after it is compressed upon entering the sensor housing, the measurand is the "recovery temperature" (T_r), which exceeds the ambient air temperature (T_a) by the amount of dynamic heating (Q):

$$T_r = T_a + Q \ . \tag{2}$$

The transfer functions determined in this section apply to the recovery temperature rather than the calculated air temperature after correction for dynamic heating. In this regard, this study differs from earlier ones. The justification, developed in later sections, is that this approach is required so that the correction for dynamic heating can be applied with proper treatment of the sensor response.

2.1 Theory

Previous studies have demonstrated that a simple first-order exponential equation with one time constant does not represent the time response of airborne temperature sensors. The suggested explanation (Lenschow, 1972) is that heat is transferred to the sensing wire of standard sensors not only from the air but also from the supporting structure that is in contact with the wire. Friehe and Khelif (Friehe and Khelif, 1992), following other prior work including that of Rodi and Spyers-Duran (1972) and McCarthy (1973), suggested representing the response with two time constants:

$$\Theta(t) = A_1 e^{-t/\tau_1} + A_2 e^{-t/\tau_2} \tag{3}$$

where $\Theta(t)$ is the normalized history of the measured temperature decaying from an initial value of one to a final value of zero. The sum of the coefficients A_1 and A_2 must then be one. The values for $\{A_1, A_2, \tau_1, \tau_2\}$ suggested by Friehe and Khelif (1992) were $\{0.65, 0.35, 0.09\,\mathrm{s}, 0.5\,\mathrm{s}\}$.

This work, following the approach of Payne et al. (1994), represents the time response of the sensor by two coupled differential equations, one that describes the response of the support on which the sensing wire is wound to the air temperature and a second that describes the response of the sensing wire to two inputs, one from the support and one from the air. No attempt is made here to determine the parameters from first principles as in Payne et al. (1994), however; instead, parameters entering the equations are determined empirically. The equations are:

$$\frac{dT_s(t)}{dt} = \frac{T_r(t) - T_s(t)}{\tau_2} \tag{4}$$

$$\frac{dT_m(t)}{dt} = \frac{a(T_r(t) - T_m(t)) + (1-a)(T_s(t) - T_m(t))}{\tau_1} \tag{5}$$

$$= \frac{\{aT_r(t) + (1-a)T_s(t)\} - T_m(t)}{\tau_1} \tag{6}$$

where $T_s(t)$ is the temperature of the support, $T_m(t)$ the measured temperature of the sensing wire, and $T_r(t)$ the true recovery temperature that is the measurand. For heat transfer to or from the wire, the parameter a then represents the fraction of the heat transferred by the air, while $(1-a)$ is transferred to or from the support. The wire responds to the combined transfers of heat with characteristic time constant τ_1 while the support structure responds to the air temperature more slowly, with time constant τ_2. It is straightforward to apply Eq. (4) and Eq. (6) to changing but not necessarily discrete conditions, so a general response to a given air-temperature history can be predicted by numerical integration of these equations. Furthermore, the equations are linear and, for constant values of the parameters, they are also time-invariant (i.e., "LTI") descriptions of the response. As a result, a particular signal for $T_r(t)$ can be decomposed into its sinusoidal Fourier components and each will satisfy these equations independently.

The first equation does not involve the measurement, so for a particular history of recovery temperature $T_r(t)$ the support temperature can be determined solely by integration of Eq. (4). Then, with $T_s(t)$ determined, Eq. (6) can be integrated to find the expected measurement $T_m(t)$ for a specified measurand history $T_r(t)$. The inverse process, finding $T_r(t)$ from the measurements $T_m(t)$, is also straightforward and only slightly more complicated, as discussed in Appendix A. These equations have analytic solutions that are sinusoidal functions if the measurand is sinusoidal. For example, if the actual recovery temperature is $T_r(t) = \sin\omega t$ where ω is the angular frequency, then the solutions for $T_s(t)$ and $T_m(t)$ are given by the following equations:

$$T_s(t) = b\sin(\omega t + \zeta) \tag{7}$$

$$T_m(t) = c\sin(\omega t + \phi) = C_1\cos\omega t + C_2\sin\omega t \tag{8}$$

where $b = (1+\omega^2\tau_2^2)^{-1/2}$, $\zeta = -\arctan(\omega\tau_2)$, and the amplitude and phase of the response are given by

$$c = \sqrt{C_1^2 + C_2^2} \tag{9}$$

$$\phi = \arctan(C_1/C_2) \tag{10}$$

with

$$C_1 = \frac{-\omega}{(1+\omega^2\tau_1^2)}\left(\tau_1 a + \frac{(1-a)(\tau_1+\tau_2)}{(1+\omega^2\tau_2^2)}\right) \tag{11}$$

$$C_2 = \left(\frac{1}{1+\omega^2\tau_1^2}\right)\left(a + \frac{(1-a)(1-\omega^2\tau_1\tau_2)}{(1+\omega^2\tau_2^2)}\right) \tag{12}$$

McCarthy (1973) used the derivative of the step-function response (Eq. (3)) to find the impulse response function and, from its Fourier transform, the sensor transfer function. That leads to the following alternate expressions for C_1 and C_2:

$$C_1 = -\omega\left(\frac{A_1\tau_1}{1+\omega^2\tau_1^2} + \frac{A_2\tau_2}{1+\omega^2\tau_2^2}\right) \tag{13}$$

$$C_2 = \left(\frac{A_1}{1+\omega^2\tau_1^2} + \frac{A_2}{1+\omega^2\tau_2^2}\right) \tag{14}$$

With $A_2 = (1-a)/(1-\tau_1/\tau_2)$ and $A_1 = 1 - A_2$, these are equivalent to the expressions for the same coefficients given by Eq. (11) and Eq. (12). This demonstrates that Eq. (4) and Eq. (6) are consistent with the step-function response given by Eq. (3) and with the equations used by McCarthy (1973) and Inverarity (2000), among others.

The transfer function $H(\omega) = c(\omega)e^{i\phi(\omega)}$ then characterizes how the sensor will respond to a unit-amplitude sine wave with angular frequency $\omega = 2\pi\nu$ where ν is the frequency. For a particular set of parameters (a=0.733, τ_1=0.0308 s, τ_2=0.447 s), characteristic of an unheated Rosemount 102E4AL sensor (hereafter called the "unheated sensor"), the amplitude response and phase delay of the transfer function are shown in Fig. 1. Similar plots of the amplitude (but not the phase) have been shown by McCarthy (1973) and Nicholls (1978). Modified transfer functions for two small changes to these parameters are also shown to illustrate the sensitivity of the solution to these parameters. This figure illustrates that serious errors will enter estimates of the sensible heat flux if temperature fluctuations at frequencies above 1 Hz make a significant contribution to the flux. The contribution to the cospectrum of temperature and vertical wind will be reduced by the product of the amplitude and the cosine of the phase such that at 10 Hz the error is about 86%, but even at 1 Hz the error is about 28%.

These equations and their solution provide a basis for correcting either the measured temperature or the sensible-heat flux calculated from the cospectrum in Eq. (1). Corrected values can be obtained by several methods including integration of the equations for the derivatives or by dividing the Fourier transform of the time series by the transfer function and then using inverse Fourier transformation to recover the corrected time series. Those correction schemes are discussed in Appendix A. To support such corrections, the next section determines the transfer function experimentally.

2.2 The response to dynamic heating

The evaluation of the time response that follows relies on the dynamic heating produced by airspeed fluctuations. These fluctuations are often significantly larger than real fluctuations in the ambient temperature. Bange et al. (2013) (cf. their Eq. 2.23) give the relationship between dynamic heating (Q) and measurable quantities as the second equality in the following equation:

$$Q = \alpha_r \frac{V^2}{2C_p} = T_r\left(\frac{\alpha_r M^2 R_a/(2C_v)}{1+\alpha_r M^2 R_a/(2C_v)}\right) \tag{15}$$

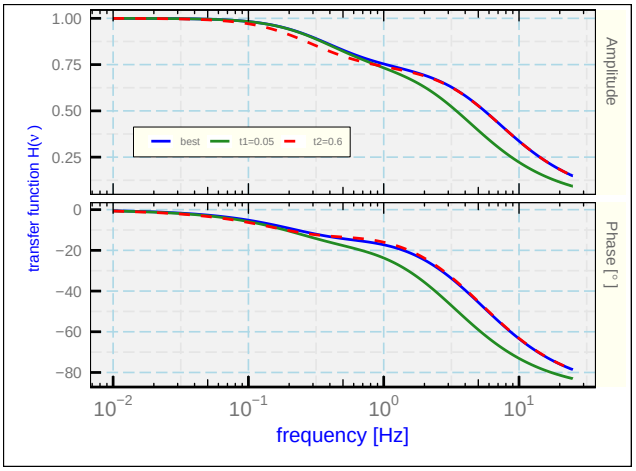

Figure 1. The amplitude and phase for the frequency domain transfer function of an unheated temperature sensor. The parameters representing that sensor, labeled "best," are a=0.733, τ_1=0.0308 s and τ_2=0.447 s. To illustrate sensitivity, the curves labeled "t1=0.05" and "t2=0.6" use instead τ_1=0.05 s and τ_2=0.6 s, respectively.

where α_r is the "recovery factor" characterizing the extent to which the air is brought to rest relative to the sensor, V is the airspeed, C_p and C_v are respectively the specific heat of air at constant pressure and constant volume. T_r is the (true) recovery temperature expressed in absolute units, M the Mach number, and R_a the gas constant for air. Because dynamic heating can exceed $20°\mathrm{C}$ at jet-aircraft flight speeds, it is often the dominant cause of fluctuations in the recovery temperature. If the fluctuations in dynamic heating are higher in frequency than those to which the sensor can respond, corresponding fluctuations will be attenuated in the measured spectrum and the phase of the measured response relative to the imposed signal will vary, from near $0°$ for fluctuations slow compared to sensor response to near $90°$ or even more for fluctuations fast compared to that response. The amplitude and phase of the recovery temperature relative to the dynamic-heating forcing therefore can be used as sensitive indicators of the response characteristics of the sensor and can constrain parameters like a, τ_1 and τ_2 that fit the differential equations to the observations. The evaluation in terms of the amplitude ratio and phase shift of the recovery temperature in response to dynamic heating will be used to characterize the transfer function and to determine if it is represented adequately by the parameterized form given by Eq. (9) and Eq. (10).

2.3 Data sources

The present investigation uses measurements from two NSF/NCAR (National Science Foundation / National Center for Atmospheric Research) research aircraft, a Gulfstream V (hereafter, GV) and a Hercules C-130. The temperature sensors producing the measurements are in widespread use so these results should have broad applicability. Some aspects of the uncertainty limits associated with these measurements of temperature are included in an NCAR Technical Note (Cooper et al., 2016), where it was estimated that the standard uncertainty in measurements of temperature from the GV is about $0.3°\mathrm{C}$. However,

this estimate does not apply when the temperature changes rapidly. Friehe and Khelif (1992) and Lawson and Rodi (1992), among others, provide reviews of the evidence for delayed response of the standard sensors. In particular, the unheated sensor referenced above has been used widely as a fast-responding sensor so it will be a focus of this study.

This research uses data archives produced by three research projects, the VOCALS (VAMOS Ocean-Cloud-Atmosphere-Land Study), CSET (Cloud Systems Evolution in the Trades) and SOCRATES (Southern Ocean Clouds, Radiation, Aerosol Transport Experimental Study) experiments. The field projects are described by Wood et al. (2011), Albrecht et al. (2019) and McFarquhar et al. (2014), respectively. All included low-level flight segments over the Pacific Ocean that are used in this paper.

2.4 Fits to the measurements

Because the airspeed V is itself conventionally determined using the processed air temperature T_a, via $V = M\sqrt{\gamma R_a T_a}$ where $\gamma = C_p/C_v$, the second expression in Eq. (15) provides the advantage that it does not rely on prior calculation of the air temperature T_a but can be calculated from only the recovery temperature T_r and the Mach number. The Mach number in turn depends only on measurements of the dynamic and ambient pressures, with a small adjustment for the water vapor pressure. However, the available measurement is not the true recovery temperature T_r but instead the measured temperature T_m, which may not include high-frequency fluctuations in T_r. This in turn affects the estimated fluctuations determined from Eq. (15). To minimize this problem, regions were sought where the fluctuations in dynamic heating were the dominant cause of fluctuations in recovery temperature. Temporarily consider these approximations: $\alpha_r \approx 1$, $R_a/(2C_v) \approx 1/5$, and M small enough thatE the denominator of the right side of Eq. (15) can be assumed equal to unity. Dynamic heating then is approximately $Q \approx T_r M^2/5$ and fluctuations in Q are related to those in T_r and M according to

$$\frac{\delta Q}{Q} \approx \frac{\delta T_r}{T_r} + \frac{2}{5}\frac{\delta M}{M} \tag{16}$$

The measured phase and amplitude of the response to the dynamic-heating term may be distorted from the correct value at frequencies where $\delta T_m/T_m$ differs from $\delta T_r/T_r$. For a representative low-level flight segment with moderate turbulence where the airspeed fluctuations were approximately consistent with an eddy dissipation rate of $3 \times 10^{-4}\,\mathrm{m^2\,s^{-3}}$, the variance of the second term in Eq. (16) is more than 100 times that of the first, indicating that the fluctuations in the first term are less than 10% of those in the second term. Therefore the right side of Eq. (15) with T_m in place of T_r was used initially to represent dynamic heating, and flight segments were used where the fluctuations in the first term were relatively small. Once a set of parameters was determined, $T_r(t)$ was calculated using the first correction procedure discussed in Appendix A. Using this revised estimate of $T_r(t)$ in place of $T_m(t)$ led to a small change in the fitted values of the parameters, but the estimate was stable after only one iteration.

2.4.1 An unheated temperature sensor

To characterize the frequency-domain transfer function of the unheated sensor, six ten-minute low level flight segments in the marine boundary layer from one flight of the NCAR/NSF C-130 in the "VOCALS" project (Wood et al., 2011) were selected that had similar flight conditions including the intensity of turbulence. The time intervals are listed in Table 1. For each flight

Table 1. Flight segments from flight 3 of the VOCALS project, 21 October 2008.

Segment	start [UTC]	end [UTC]
1	6:50:00	7:00:00
2	7:33:00	7:43:00
3	10:46:00	10:56:00
4	11:42:00	11:52:00
5	12:43:00	12:53:00
6	13:30:00	13:40:00

segment, the phase and amplitude ratio between the measurement and the dynamic heating term were calculated and the results for all six segments were averaged in 200 logarithmically spaced intervals in frequency. The results for the average phase are shown in Fig. 2a. The theoretical curve is based on best-fit parameters as determined from these measurements and those of the amplitude ratio, discussed next.

The ratio of the amplitude of the response to that of the dynamic-heating signal, used as an estimate of the gain of the transfer function, is shown in Fig. 2b. It is useful to consider both the amplitude and phase when determining the response parameters because, as shown in Fig. 1, the amplitude of the transfer function is more sensitive to τ_2 than the phase but τ_1 is a very sensitive predictor of the phase at high frequency. For the set of favored parameters, Fig. 2b shows the standard prediction and another with τ_2 set to $0.6\,\mathrm{s}$ instead, to show the sensitivity of this result to that parameter. The best prediction based on the measured phases consistently underestimates the ratio of spectra for frequencies below about $0.1\,\mathrm{Hz}$ and above about $3\,\mathrm{Hz}$ but is reasonably consistent with the observed ratio between those limits. Below $0.1\,\mathrm{Hz}$ variance spectra indicate that the sensor is responding to real fluctuations in temperature not attributable to dynamic heating, as would be expected at these low frequencies. Above $3\,\mathrm{Hz}$ the prediction is much too low, probably because there is noise or other spurious variance in $T_m(t)$ not caused by dynamic heating.

The fit procedure used Eq. (9) and Eq. (10) to find the theoretical value of the amplitude ratio and phase at each frequency represented in the observations. For assumed values of the three parameters a, τ_1 and τ_2, a chi-square was calculated from the differences between these theoretical values and the observed values. The frequencies used for the fit were 0.01 to $12\,\mathrm{Hz}$ for the measurements of phase and 0.1 to $3\,\mathrm{Hz}$ for the measurements of amplitude ratio, to avoid regions where effects other than dynamic heating appear to bias the measurements. Then a search procedure varied these parameters to seek the minimum value of the chi-square. The resulting values were a= 0.73, τ_1= 0.031 and τ_2= 0.45. The chi-square for the fit is about 18 times larger than expected if the fit represents the measurements to measurement uncertainty, so it is difficult to assign uncertainty limits to this result on the basis of this fit because of this not-understood excess chi-square, but the fit minimum distinguished nearby values to about three significant digits in all three parameters. The Hessian from the fit implies that the results with standard uncertainties are a= 0.733 ± 0.004, τ_1=$0.0308 \pm 3 \times 10^{-4}\,\mathrm{s}$ and τ_2=$0.45 \pm 0.02\,\mathrm{s}$.

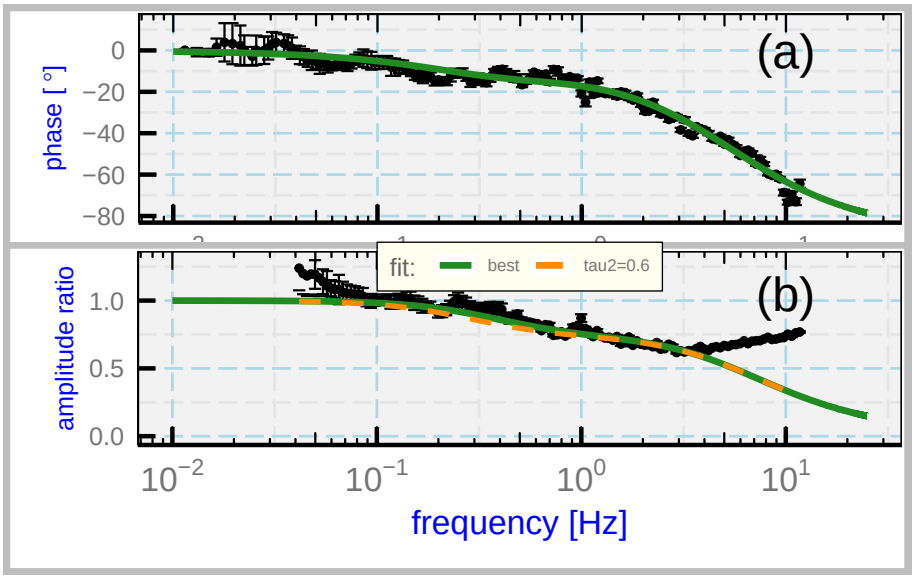

Figure 2. (a): Phase of measured recovery temperature relative to dynamic heating, for the measurements (with error bars) and for the theoretical response for the best-fit parameters (green line). The error bars indicate two-standard-deviation ranges in the mean at each plotted point. Data from the flight segments listed in Table 1.

(b): The ratio of the spectral amplitude for the measurement of recovery temperature ($T_m(t)$) to that for dynamic heating (Q), shown as the plotted data points. There are additional data points at frequencies below about 0.04 Hz that do not appear in this plot because they lie above the upper limit for the ordinate. The green line is the prediction from the transfer function determined from the best-fit values matching the phase lag between these variables, and the dashed orange line is a similar result with the second time constant τ_2 increased from 0.447 to 0.6 s to illustrate sensitivity to this parameter.

To complete the iteration discussed earlier, the measured recovery temperature was then corrected as described in Appendix A, using the parameters from this first fit, to find a prediction for the actual recovery temperature $T_r(t)$. After recalculating Q using Eq. (15) with that estimate of $T_r(t)$ in place of $T_m(t)$, the calculation of phase and amplitude was repeated and the results were fitted again by adjusting the fit parameters. Only insignificant changes, much smaller than the quoted uncertainties, resulted from this iteration.

2.4.2 Heated sensors

Measurements from two slower sensors, a heated Goodrich/Rosemount 102 sensor and a similar Harco Model 100009-1 Deiced TAT sensor, have also been evaluated, but only the latter (hereafter called the "heated sensor") is discussed here because they have similar response. The spectral variance for both these measurements has apparent rapid attenuation beginning at about 0.1 Hz, as shown in Fig. 3, and the response is attenuated seriously above about 1 Hz. To find the transfer function for this

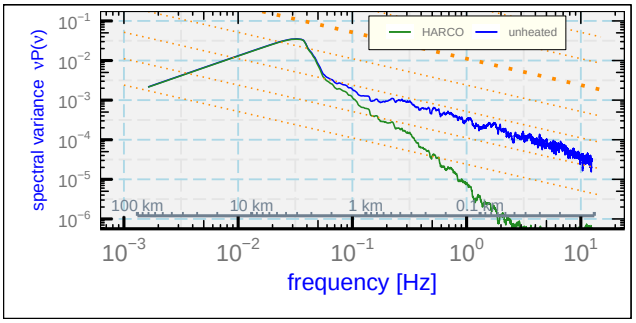

Figure 3. Spectral variance $P(\nu)$ weighted by frequency (ν) for the recovery temperature measured by a heated and an unheated temperature sensor.

Table 2. Flight segments used to determine the response characteristics of a heated sensor.

Project / Flight	start [UTC]	end [UTC
CSET / 5	2015-07-14 17:52:00	18:02:00
CSET / 5	2015-07-14 19:45:30	19:55:30
CSET / 5	2015-07-14 20:37:17	20:47:17
SOCRATES / 15	2018-02-24 5:52:00	6:02:00
SOCRATES / 15	2018-02-24 6:05:00	6:15:00

sensor, boundary-layer flight segments from the SOCRATES and CSET projects were compiled into one data set from the flight periods shown in Table 2.

Attempts to use the same three-parameter representation of the transfer function relative to dynamic heating led to unsatisfactory fits, apparently because fluctuations caused by dynamic heating were not as dominating a cause of the temperature fluctuations as they were in the measurements from VOCALS used for the unheated sensor, so a different approach is used here. Because the evaluation in Sect. 2.4.1 provides a good representation of the unheated sensor, the measurements from that sensor, corrected as described in Appendix A, were used as the reference for the assumed-correct recovery temperature. Then the phase and amplitude ratio were found for the transfer function required to produce the heated-probe measurements from the unheated-probe measurements. This did not require any assumptions about equations or parameters determining the transfer function.

The measured phase and amplitude ratio for this data set are shown in Fig. 4. The fits for the response function defined by Eq. (9) and Eq. (10) are shown as the blue lines labeled "3-par" in that figure. The fitted values for $\{a, \tau_1, \tau_2\}$ were $\{0, 0.108\,\mathrm{s}, 1.28\,\mathrm{s}\}$, and to obtain this result the fit had to be constrained to keep a non-negative. A value of zero for the parameter a would indicate that no heat is transferred from the sensing wire to the air, but instead all is transferred to the support which has a relatively slow characteristic response.

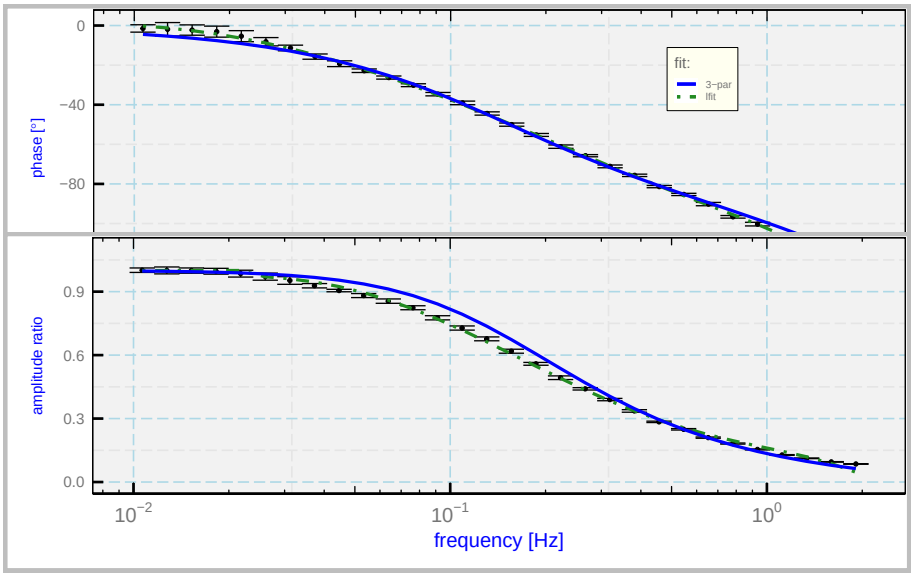

Figure 4. The phase (top) and gain (bottom) for the transfer function characterizing a heated temperature sensor. The measurements are indicated by error bars that show two-standard-deviation limits from the mean value). Two fits to the measurements, one based on the three-parameter representation ("3-par") and one on a polynomial fit ("lfit"), are described in the text.

The three-parameter fit is not consistent with the measurement errors even though it provides an approximate representation of the transfer function. The apparent reason is that there is conflict between the constraints imposed by the amplitude ratio and the phase, such that either could be represented reasonably but not both. Because the three-parameter fit distorted the measured result, fits in the logarithm of the frequency were used to provide a better representation of the measurements, as shown by the dashed green lines labeled "lfit". Those fits are given by these equations and coefficients, with $x = \log_e(\nu/\nu_0)$ where ν is the frequency, $\omega = 2\pi\nu$ and ν_0=1 Hz:

$$\text{for } \nu > 0.024\,\text{Hz}, \quad H(\omega) = (h_0 + h_1 x + h_2 x^3 + h_3 x^4 + h_4 x^5) e^{i\phi(\omega)} \tag{17}$$

$$\text{for } \nu \le 0.024\,\text{Hz}, \quad H(\omega) = 1 \tag{18}$$

$$\text{for } all\ \nu, \quad \phi(\omega) = p_0 + p_1 x + p_2 x^2 + p_3 \arctan(\nu/\nu_0) \tag{19}$$

The coefficients obtained by fitting to the observations are h_{0-4}={0.124, −0.116, −0.0929, −0.0374, −0.00391} and p_{0-3}= {−190.3, −78.7, −8.16, 90.3}. This fit (with negative-frequency values defined as the complex conjugate of the values at the corresponding positive frequency) represents the transfer function better than the three-parameter fit, although the fit must be modified above about 2 Hz because those values were not constrained by the measurements. A suggested modification is to

Table 3. Parameters for the time response of available temperature sensors on the NSF/NCAR aircraft, adjusted to $Z = 0.3$. For other conditions, scale as represented for τ_1' in Eq. (20). Parameters for the unheated sensor were also determined for measurements on the GV, with the result 0.73, 0.035, 0.36, but the fit was less satisfactory than the one for the C-130 so the fit in the table has been used in this paper.

sensor	a	τ_1 [s]	τ_2 [s]
"unheated" (Rosemount 102E4AL on C-130)	0.73	0.031	0.45
"heated" (HARCO Model 100009-1 Deiced TAT)	0.0	0.13	1.28

duplicate the value at 2 Hz to higher frequencies; this appears to be adequate because there is so little variance measured by this sensor at these frequencies, as shown by Fig. 3.

2.4.3 Expected dependence on flight conditions

Based on measurements in a wind tunnel, Stickney et al. (1994) indicated that the fast-response characteristic time τ_1 for the unheated sensor varies approximately as $\log(Z^{-0.68})$ where $Z = M\rho_a/\rho_s$ with M the Mach number, ρ_a the air density and ρ_s the air density under standard conditions. The mean value of Z for the flight segments used to find the best-fit parameters for the unheated sensor on the C-130 was $Z = 0.3$, so this suggests that the first characteristic time for that sensor is best represented by

$$\tau_1'(Z) = \tau_1 \left(\frac{0.3}{Z} \right)^{0.68} . \tag{20}$$

For a flight segment at about $11.5\,\mathrm{km}$ altitude, where the mean value of Z was 0.228, τ_1 was found to be $0.037\,\mathrm{s}$, exactly matching the prediction of (20), so this provides some limited support for that equation. For these reasons, the values of τ_1 found in preceding sections have been adjusted to a reference value of $Z = 0.3$ in Table 3. For other conditions, it is suggested that the best estimate will be to multiply τ_1 by $(0.3/Z)^{0.68}$.

2.5 Response to a step change

Previous studies have mostly used sharp temperature changes in the atmosphere, for example from climbs through the inversion at the top of a boundary layer, to study the time response. A search of representative VOCALS climbs and descents through inversions capping the marine boundary layer found that almost all have measurable structure and are not discrete transitions, but there was one near-ideal example. Figure 5 shows the time history of the measured temperature for $8\,\mathrm{s}$ from VOCALS flight 3, when the aircraft descended through the top of the marine boundary layer at approximately $5\,\mathrm{m\,s^{-1}}$. The temperature structure in this case was remarkably consistent with a near-constant temperature above the inversion and a near-adiabatic temperature structure below the inversion.

The suggested measurand history, if the discontinuity at the inversion is discrete, is that shown by the dashed black and red lines. The predicted time response from Eq. (6) for the time constants listed in Table 3 for the unheated sensor (adjusted for air

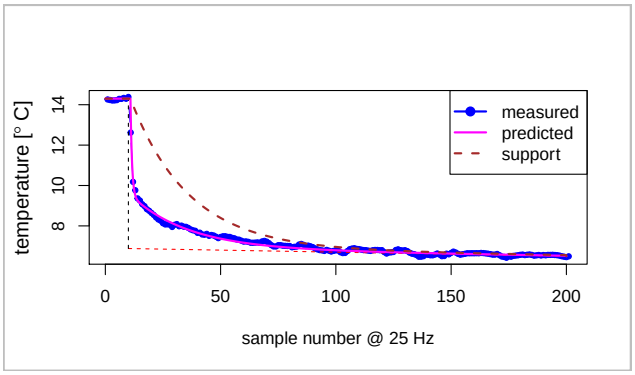

Figure 5. (blue dots): Temperature measured at 25 Hz during descent through an inversion capping the marine boundary layer, from VOCALS flight 3, starting at 8:13:50 UTC. The dashed red line shows a dry-adiabatic lapse rate in the marine boundary layer, and the dashed black line is a reference line indicating the location of the top of the boundary layer. The prediction using the parameters listed in the text is shown as the magenta line, mostly over the blue dots representing the measurements. The dashed brown line is the calculated temperature of the support that contacts the sensing wire.

density and flight speed) is shown as the magenta line in Fig. 5. The predicted response is consistent with the observations and supports the approximate validity of the parameters determined from fits to the response to dynamic heating.

2.6 Uses of the transfer functions

The transfer functions have two potential uses: (i) to predict how airborne thermometers will respond; and (ii) to correct measurements to compensate for the time response of the sensors. The two sections that follow are examples of these two uses. In the next section, the transfer functions are used to assess how sensors respond to dynamic heating and to develop appropriate correction schemes. Then the following section applies the transfer functions to improve measurements of the flux of sensible heat.

3 Correcting for Dynamic Heating

In conventional processing to calculate the ambient air temperature, an independently determined estimate of dynamic heating is subtracted from the measured temperature. As described in Sect. 2.2, when the sensor cannot respond to fluctuations in dynamic heating, this procedure introduces errors and excess noise into the resulting air temperature. Data processing should instead apply a correction that represents how dynamic heating affects the measurement from the sensor, not how it affects the recovery temperature.

The approach followed here is to filter the dynamic-heating term so that only the actual sensor response to dynamic heating is subtracted from the measurement. This is made possible by the assumed linearity in response of the sensor, which is required if this part of the response is to be separated from the more general response to the combination of dynamic heating and true

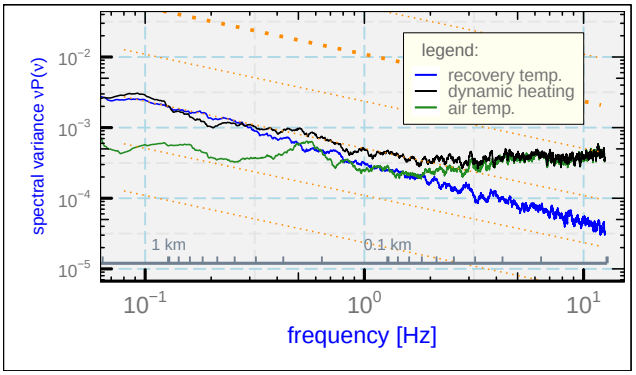

Figure 6. The weighted variance spectrum as a function of frequency ν for the recovery temperature measured by an unheated sensor. The spectra for the dynamic-heating term and for the calculated air temperature after this correction is applied are also shown.i

fluctuations in temperature. This filtering removes a significant source of erroneous fluctuations present in many temperature measurements made from research aircraft.

Figure 6 illustrates the problem. The measurements are from a low-level flight segment over the ocean where other indications are reasonably consistent with an inertial subrange. The slope of the temperature variance spectrum (log spectral variance vs log frequency) would be expected to be -5/3 (or -2/3 in this plot where the spectrum is multiplied by the frequency). The variance spectrum of the measured recovery temperature has a steeper slope than this, as expected if the time response attenuates the signal at higher frequencies. However, the variance spectrum for the estimated ambient temperature appears to have a substantial amount of high-frequency contamination. This matches the high-frequency portion of the spectrum for dynamic heating. If the sensor measured the correct recovery temperature, its spectrum should exceed that of the ambient temperature (as is the case around 0.1 to 0.5 Hz) so that the subtraction of dynamic heating would produce smaller variance in the measured ambient temperature.

The filtered response has been obtained from the transfer function in several equivalent ways, by integration of the differential equations applied to Q, by Fourier transforms using the transfer function, and by applying a digital filter designed from the transfer function, all with almost equivalent results. The filtered dynamic-heating adjustment will be denoted Q', and the calculated air temperature then becomes

$$T'_a(t) = T_m(t) - Q'(t) \tag{21}$$

instead of Eq. (2).

Figure 7a shows the variance spectra that result from all three methods when applied to measurements from an unheated sensor. The modified variance spectrum obtained by integration of the underlying differential equations is shown as the orange line labelled “DiffEq”. The dynamic-heating correction is appropriately attenuated at high frequency after this integration. The results obtained after application of a digital filter representing the transfer function, labeled “filter”, or after Fourier transformation, labelled “FFT”, are overlapping so as to be indistinguishable in this plot. These corrected estimates of the

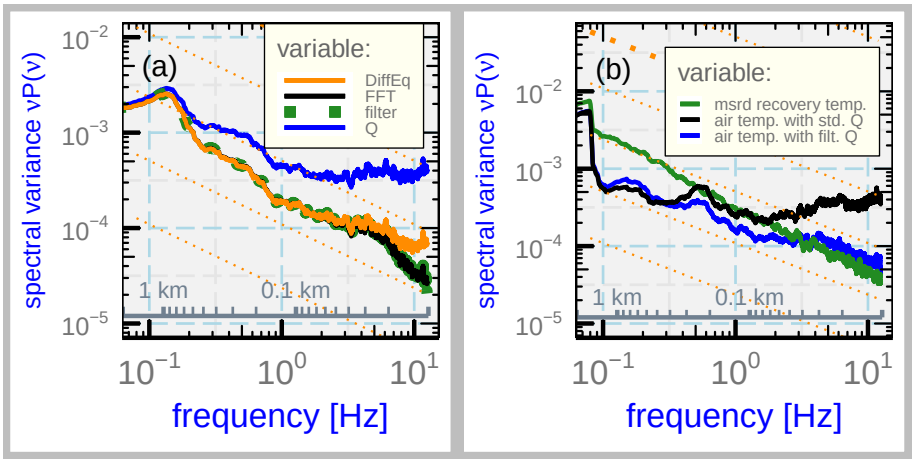

Figure 7. Variance spectra for an unheated sensor, for the same flight segment used for Fig. 6.

(a): The dynamic-heating term ("Q") and the filtered term obtained by integrating the differential equations for the derivatives ("DiffEq"), by Fourier transformation with application of the transfer function ("FFT"), or applying the digital filter ("filter"). The result for the latter is so close to that for "FFT" that it is obscured in this plot.

(b): The measurement of recovery temperature and ambient temperature calculated using the filtered dynamic-heating term. The original variable for ambient temperature based on standard processing ("with std Q") is also shown.

dynamic heating are attenuated even more than the result from numerical integration and are in better agreement with the predicted effect of the transfer function, which for example predicts attenuation of the variance spectrum by a factor of 0.096 for the component with frequency 10 Hz. The numerical integration was closer to the results of the filter after the measurements were interpolated to 125 Hz with 25 Hz smoothing, integrated, and then resampled to obtain 25 Hz measurements, so the high-frequency discrepancy appears to result from accumulating numerical errors in the integration. The equivalence of the results from the digital filter and from Fourier transformation with application of the transfer function supports the validity of these results and suggests that these are preferable and equivalent methods for filtering dynamic heating to match the response of the temperature sensor.

A revised estimate of the ambient air temperature was calculated using Eq. (21) and the corrected dynamic-heating term Q'. The spectral variance for this air temperature, shown in Fig. 7b as the blue line, is improved considerably at high frequency vs. that using the standard correction.

```
## Warning in sqrt(ar2H - arH^2): NaNs produced
```

In the case of the heated sensors, the revision is still more significant because they respond more slowly. Figure 8a shows the result of filtering the dynamic-heating term for a heated sensor. The result of integration ("DiffEq") and the digital filter ("filter") are almost identical so there is no evidence of the numerical problems that were encountered with the integration for the unheated sensor. The difference vs. the original is quite dramatic even at 1 Hz, and the errors are significant for all

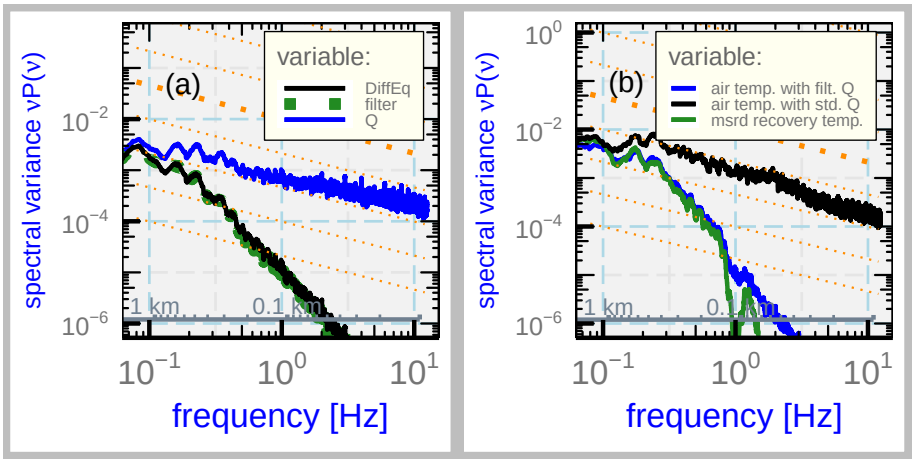

Figure 8. Variance spectra for a heated temperature sensor.

Left, (a): The unmodified dynamic-heating term ("Q") and the two filtered terms. The results from solving the differential equations ("DiffEq") or from application of the digital filter ("filter") are overlapping and indistiguishable in this figure.

Right, (b): The air temperature as modified by filtering the dynamic-heating term (blue line). The other plotted spectra are for the measured recovery temperature and the air temperature with the conventional dynamic-heating correction.

frequencies above about 0.1 Hz. Because either corrected variance spectrum represents how the temperature sensor responds to the actual fluctuations, subtracting the actual fluctuations in dynamic heating instead of the filtered fluctuations introduces substantial erroneous variability into the calculated air temperature.

Figure 8b shows how this affects the spectral variance of the measured air temperature. The slow response of this sensor causes the measured recovery temperature (green line) to have very low spectral variance when the frequency is above 1 Hz, so the variance in the standard air-temperature measurement in this frequency range is almost entirely caused by erroneous adjustment for fluctuations in dynamic heating to which the sensor does not respond. The correction procedure using a filtered dynamic-heating correction removes this excess spectral variance and produces a signal where the variance for frequencies above about 0.1 Hz arises primarily from variance in the measured recovery temperature. The variance spectrum for the conventionally processed temperature looks approximately as might be expected in an inertial subrange, but the variance above about 0.5 Hz is a false signal that does not arise from real variance in temperature. It therefore becomes very important to use this revised processing scheme to avoid erroneous measurements even for changes occurring over 5 s or more. The reasonable appearance of the variance spectrum for the standard result is misleading because the measurement is not responding to real fluctuations in air temperature at high frequency. The measurement with filtered dynamic heating is a better indication of the measured fluctuations.

Fig. 9a illustrates the removal of erroneous structure by filtering for the unheated sensor, and Fig. 9b shows a similar example for the heated sensor. These figures illustrate that the erroneous fluctuations in the uncorrected measurements can be important

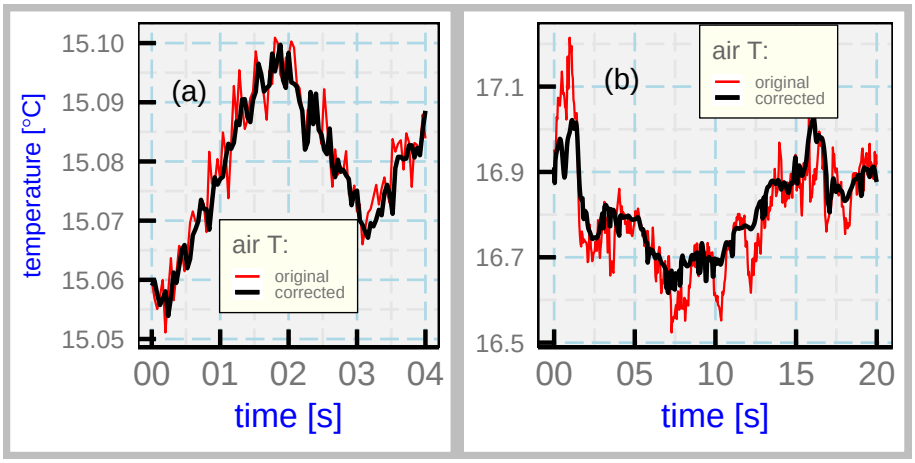

Figure 9. Comparison of the original calculated air temperature and the same temperature after filtering the dynamic-heating correction: (left): An unheated sensor; (right): A heated sensor.

in many potential uses of these measurements and should be removed as part of standard processing. The effect is particularly significant for the heated sensor, for which the conventionally processed temperature has large fluctuations that are caused by subtraction of fluctuations in dynamic heating to which the sensor does not respond. These do not arise from real fluctuations in ambient air temperature.

4 The Flux Density of Sensible Heat

4.1 Outline of the correction procedure

Most past studies of temperature-sensor response (e.g., McCarthy (1973), Nicholls (1978), Inverarity (2000)) applied corrections to the air temperature after correction for dynamic heating. That applies the full correction for dynamic heating Q without considering that the sensor may respond only partly to high-frequency fluctuations in Q, which was shown in Sect. 3 to lead to erroneous noise in the air temperature. Then that noise is amplified by the correction procedure. These errors are avoided if corrections are applied instead to the measurement of the recovery temperature. Then the amplification of signals by application of the transfer function restores the fluctuations produced by dynamic heating, and those fluctuations are then removed by subtracting the measured dynamic heating term from the corrected recovery temperature.

The eddy-correlation calculation used here starts with the Fourier representation of the measured recovery temperature. (Fourier transforms are denoted here by the symbol "$\hat{}$" over variables.) The measurement is related to the true recovery temperature via $\hat{T}_m(\nu) = H(\nu)\hat{T}_r(\nu)$ where $H(\nu)$ is the frequency-domain transfer function. The true recovery temperature will be the inverse Fourier transform of $\hat{T}_r = \hat{T}_m(\nu)/H(\nu)$. The Fourier representation of the air temperature is then obtained from $\hat{T}_a = \hat{T}_m(\nu)/H(\nu) - \hat{Q}(\nu)$, which includes both the correction for time response and the subtraction of dynamic heating.

Multiplication by the complex conjugate of the Fourier representation of the updraft then gives the cospectrum representing the flux of sensible heat, with an appropriate scale factor as specified in Eq. (1). The resulting cospectrum is then integrated over an appropriate wavelength range to produce the measured flux density of sensible heat. This will normally exclude wavelengths greater than a few kilometers so that the estimate represents the turbulent contribution.

4.2 Examples of Measured Cospectra and Fluxes

Two examples of measured cospectra illustrate the effect of the correction. The first example is from the SOCRATES project, 24 January 2018, 6:00:00 to 6:15:00 UTC, and the second is from the CSET project, 1 August 2015, from various segments from 16:00:00 to 19:15:00 UTC. The flight segments were all at low level ($150\,\mathrm{m}$) in the marine boundary layer over the Pacific Ocean. An unheated sensor was used to measure temperature on these flights. In each case, the cospectra from three flight segments of $5\,\mathrm{min}$ (SOCRATES) or $10\,\mathrm{min}$ (CSET) duration were averaged to produce the measured cospectra. Uncertainties in this measurement and common features of the atmospheric boundary layer are discussed by Lenschow (1995). Lenschow and Stankov (1986) suggested that, for 10% uncertainty in a measurement of scalar flux, an averaging distance of 100–500 times the boundary-layer height is required. (See also Lenschow et al. (1994).) The flight segments in these two cases span about 80–150 times the boundary-layer height, so they are marginal by this criterion, but the measurements still serve to illustrate the effect of the proposed correction.

The corrected cospectra are shown in Fig. 10. This plot format is unconventional so some explanation is provided here. The cospectrum can be positive or negative, so it is usually plotted using a linear ordinate scale. However, the range of ordinate values is displayed better with a logarithmic scale, even after weighting the cospectrum by frequency. The compromise made in this plot is to use a logarithmic scale but plot negative values with sign reversed and with a different color, here red instead of blue. Other features of this plot and computation conventions include the following:

1. The cospectra have been smoothed using Daniell smoothing, with consecutive smoothing using width-3 for frequencies above $0.01\,\mathrm{Hz}$, then width-5 for frequencies above $0.1\,\mathrm{Hz}$, then width-17 for frequencies above $1\,\mathrm{Hz}$. For these $5\,\mathrm{min}$ flight legs and for $25\,\mathrm{Hz}$ measurements, the maximum smoothing interval is about $0.05\,\mathrm{Hz}$ so most spectral features are retained even with this strong smoothing. Additional smoothing results from averaging three cospectra to obtain the plotted values.

2. Further smoothing is included by binning the results into 100 logarithmically spaced intervals in frequency and averaging in those bins. That results in the blue dots (or dark red dots for negative points).

3. The listed "total" flux is that arising from the part of the flux with frequency above $0.01\,\mathrm{Hz}$. This frequency limit restricts the calculation to wavelengths smaller than about $13\,\mathrm{km}$. Another measurement of the flux is calculated for wavelengths below $2\,\mathrm{km}$. That or a still smaller wavelength limit is a reasonable measure of the part of the flux contributed by turbulent air motions in the boundary layer, so that second measurement is used as the primary measurement in this study.

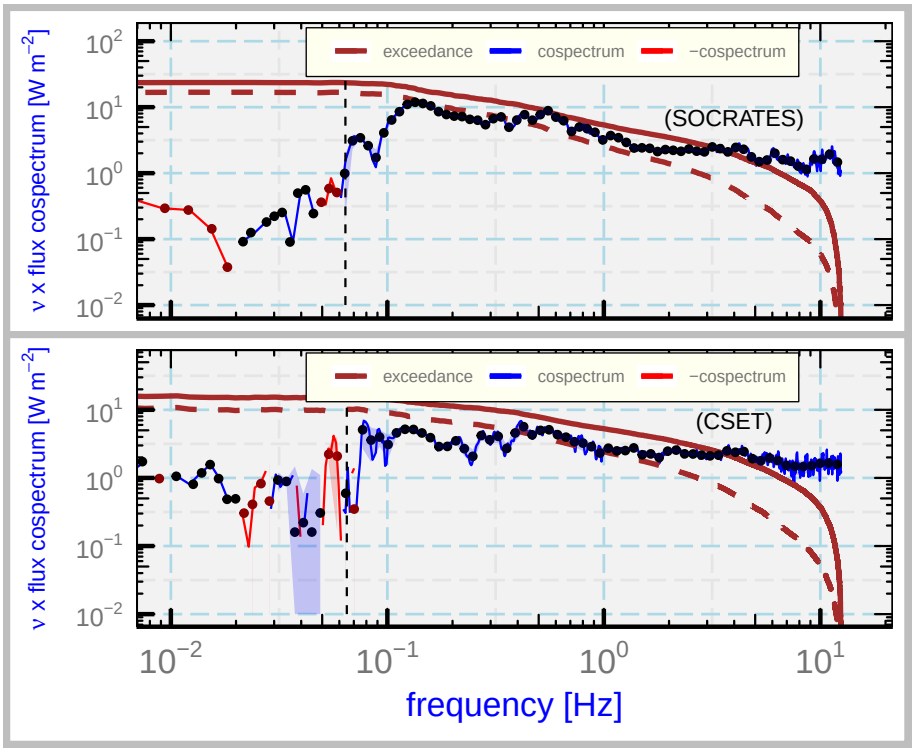

Figure 10. The corrected flux of sensible heat, weighted by the frequency ν, for low-level flight segments over the Pacific Ocean. The "exceedance" is the complement of the cumulative distribution function (i.e., the sum of contributions from frequencies above the plotted value), and the dashed brown exceedance line is that without transfer-function correction but with adjustment of the dynamic-heating term to incorporate the estimated response of the temperature sensor. For the SOCRATES example, the total flux is $23.6\,\mathrm{W\,m^{-2}}$ and the flux contributed from wavelengths smaller than $2\,\mathrm{km}$ is $23.5\,\mathrm{W\,m^{-1}}$, while the corresponding numbers for the CSET example are 16.0 and $15.4\,\mathrm{W\,m^{-2}}$. The dashed black line shows the frequency limit that corresponds to a wavelength of $2\,\mathrm{km}$.

4. The brown line labeled “exceedance” is a cumulative distribution function for the cospectrum, called “exceedance” because it is the contribution from all frequencies *higher* than the indicated value. (This has been called the “ogive” by, e.g., Foken et al. (2006).) At high frequency on a logarithmic scale, where some of the most interesting variation is located, the exceedance distribution is more informative that the conventional cumulative distribution. Its units are $\mathrm{W\,m^{-2}}$, not $\mathrm{W\,m^{-2}}$ per logarithmic interval as is the case for the weighted cospectrum.

The exceedance distributions before correction, shown as the dashed brown lines, were calculated using a dynamic-heating correction that was filtered to match the response of the sensor, but otherwise were not corrected. Without correction for the response as represented by the transfer function, about 33% of the flux contributed by wavelengths smaller than $2\,\mathrm{km}$ would be missed. The underestimation is particularly serious at higher frequencies: In both cases the measured contribution from

frequencies above 1 Hz is more than twice as large after correction as it is without correction. A significant contribution to the error is the phase shift that causes the measured temperature to be shifted in phase relative to the updraft, as shown in Fig. 1.

Lawson and Rodi (1992) estimated that, in comparison to their fast thermocouple sensor, the unheated Rosemount sensor underestimated the flux by about 21% in their measurements. The magnitude of the correction here is larger than that estimated error, but the flight speed of the aircraft was about 30% higher in this case so a larger error would be expected.

Because the corrected cospectrum appears realistic at frequencies of 1 Hz and above, it is possible to judge if the frequency coverage is adequate. In this case, the exceedance curve is less than 2% at 10 Hz and falls rapidly above that frequency, even after correction, so it appears likely that additional contributions from higher frequencies can go unmeasured without introducing serious errors into the measurement of flux. Additional guidance regarding the expected shape of the cospectrum and the required frequency response is provided by Lenschow (1995). The generalized cospectra provided there suggest that, for flight at $130\,\mathrm{m\,s^{-1}}$, frequencies up to about 1.3 Hz–10 Hz, depending on altitude, must be measured. The higher frequency limit applies to low-level flight at about $30\,\mathrm{m}$ above the surface. Those results suggest that, if the measurements are corrected as suggested here, reliable measurements of sensible-heat flux can be made with the unheated sensor.

4.3 Evidence from Simulated Measurements

As a test of the approach described in the preceding section, a simulated case was analyzed in the same way. Time series were generated representing isotropic wind measurements by starting with a Gaussian-noise spectrum, weighting the Fourier components to obtain a $-5/3$ slope, and then using an inverse Fourier transform to reconstruct the simulated measurement series.

A time series for temperature was generated similarly but scaled by a factor of $0.2^{\circ}\mathrm{C\,m^{-1}\,s}$, and then a correlation of 0.3 was introduced between temperature and updraft fluctuations. In this simulation, about 15% of the flux from wavelengths below $2.5\,\mathrm{km}$ is contributed by frequencies above 1 Hz, where the sensor may respond incompletely to the fluctuations and underestimate the flux.

Figure 11 shows (as the green line) how the simulated cospectrum would be measured by a sensor with response parameters $\{a, \tau_1, \tau_2\}$ equal to $\{0.733,\ 0.0308\,\mathrm{s},\ 0.447\,\mathrm{s}\}$, as is characteristic of an unheated sensor. The simulated measurement of air temperature was obtained by adding the dynamic-heating correction to the simulated air temperature and then applying the digital filter developed in Sect. 3 to estimate how the sensor would respond. Then the resulting value for measured recovery temperature was corrected for dynamic heating to obtain the value that would be measured for the air temperature, and that value was used with the simulated updraft to calculate the cospectrum. The resulting measured cospectrum is significantly smaller than the generated cospectrum for frequencies above about 1 Hz and is almost a factor of ten too low at 10 Hz. The measured exceedance distribution (dashed brown line) emphasizes the extent of the missing flux at high frequency.

The cospectrum obtained using the correction procedure of Sect. 4.1 is consistent with the generated cospectrum, as illustrated by the corrected exceedance distribution in Fig. 11 (dashed black line). For wavelengths smaller than $2.5\,\mathrm{km}$, the generated flux of sensible heat is $39.5\,\mathrm{W\,m^{-2}}$ and the measured values before and after correction are 33.2 and $38.5\,\mathrm{W\,m^{-2}}$. The correction thus reduces the 15% measurement error to about 2.5%. The representation of the high-frequency contribution

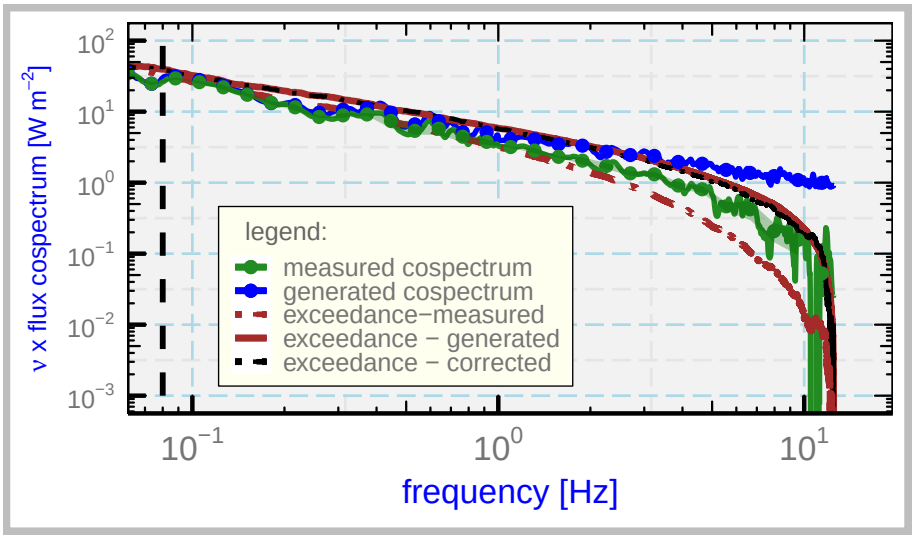

Figure 11. The cospectrum for the flux of sensible heat (blue line), weighted by frequency ν, for the simulated data generated as described in the text. Three $10\,\mathrm{min}$ segments of simulated $25\,\mathrm{Hz}$ data were averaged. The measured cospectrum was obtained by filtering the simulated recovery temperature and subtracting the correction for dynamic heating. For the generated and measured cospectrum, filled circles indicate the average values calculated in 50 logarithmically space intervals, and for the measured cospectrum shading indicates the standard deviation in those intervals. The exceedance lines show the contribution to flux from frequencies higher than the plotted frequency. The corrected cospectrum is not shown but is consistent with the generated cospectrum, as demonstrated by the agreement between the generated exceedance and the corrected exceedance. The units for the exceedance distributions are $\mathrm{W\,m^{-2}}$, while the units for the weighted flux cospectra are $\mathrm{W\,m^{-2}}$ per unit logarithmic increment.

is improved significantly by the correction procedure: For the contribution to the flux from frequencies above $3\,\mathrm{Hz}$, the respective values for the generated, measured, and corrected exceedance distributions are 15.3, 10.8, and $15.1\,\mathrm{W\,m^{-2}}$, so about 30% of the contribution in this frequency range would be missed without correction.

This test only confirms consistency between the prediction of the transfer function and the correction procedure based on that function. The former, when deployed in a digital filter, is dependent on the assumptions and weaknesses in that filter, while the latter may be influenced by end effects and window effects from calculating the Fourier transforms. The agreement between the simulated and corrected flux therefore provides some support for the filter developed in Sect. 3 and for the correction procedure developed in this paper.

5 Conclusions

The key findings are these:

1. The differential equations Eq. (4) and Eq. (6) provide an analytical representation of the transfer function for the recovery temperature measured by an unheated sensor. With appropriate values of the parameters, that analytical transfer function was consistent with the phase and gain of the measured response to dynamic-heating fluctuations. This is evidence that the equations provide a valid representation of the time response for that sensor. The predictions of the equations are less satisfactory when applied to heated sensors, possibly indicating incomplete representation of the transfer of heat to those slower sensors.

2. For the unheated Rosemount 102E4AL sensor, the three parameters in those equations (characterizing the two time constants and the fraction of heat transfer to the air vs. that to the structure supporting the sensing wire) can be determined with small uncertainty by fitting the transfer function to observations of dynamic heating. These parameters are thus constrained well and can be relied upon to make corrections to the measurements and otherwise to characterize the effects of time response of that sensor.

3. The transfer function for the unheated sensor can then be used to estimate the true recovery temperature. Transfer functions for other sensors then can be determined by comparison to that estimate of the measurand to which they are responding. This approach has been used here for the slower heated sensors and should provide a means of correcting other sensors slower than the unheated sensor. Appendix A uses these results with standard methods to correct the measurements from airborne temperature sensors for their time response.

4. Because temperature sensors often do not respond fast enough to measure high-frequency components of the dynamic-heating correction, erroneous fluctuations are introduced by conventional data processing when the full dynamic-heating term is subtracted. Instead, that term should be filtered to match the response of the temperature sensor. A digital filter is proposed that can be used to correct standard processing schemes to eliminate the errors arising from the dynamic-heating term. The errors discussed here are prevalent in almost all existing data from research aircraft, so application of this proposed correction method would lead to significant improvement in those measurements.

5. An algorithm was proposed for calculating sensible-heat flux that uses the transfer function to correct the measured cospectrum. Two illustrative cases were presented in which there was significant correlation between temperature and updraft at a range of frequencies including those above 1 Hz. The measured values of sensible-heat flux would be underestimated significantly (by about 33%) without correction.

6. The cospectrum with correction appears to be represented reasonably at frequencies up to about 10 Hz, so the decrease in the cospectrum with frequency near that value suggests that it is not necessary to measure contributions from still higher frequencies. This conclusion is tentative and needs reconsideration when applied to new cases.

7. Results of a simulation support the consistency between the response as represented by the digital filter and the application of the transfer function to correct the measurement of the flux of sensible heat.

Appendix A: Correcting the Temperature

The true recovery temperature T_r can be retrieved from the measured temperature T_m in two ways, either from the differential equations or by Fourier transformation. Only a cursory discussion of these techniques is included here because the procedures are standard and follow earlier work, notably that of Inverarity (2000) and Foster and Chan (2012).

The differential equations Eq. (4) and Eq. (6) involve two unknowns, the actual recovery temperature $T_r(t)$ and the temperature of the supporting structure $T_s(t)$. The second equation can be used to eliminate T_r from the first:

$$\frac{dT_s(t)}{dt} = \frac{\frac{1}{a}\left\{\tau_1 \frac{dT_m(t)}{dt} + T_m(t) - (1-a)T_s(t)\right\} - T_s(t)}{\tau_2} \tag{A1}$$

Because the measured temperature $T_m(t)$ is known, this can be integrated from an assumed initial value $T_s(0)$ to find the temperature of the support, $T_s(t)$. Then Eq. (6) can be solved to give the true recovery temperature $T_r(t)$ without further integration. The only choices to be made are the numerical method used to find the derivative dT_m/dt (here centered fourth-order) and the integration method applied to Eq. (A1), here fourth-order Runge-Kutta integration with Cash-Karp (Cash and Karp (1990)) adjustment of the step size. If a centered second-order finite-difference expression is used for $dT_m(t)/dt$ and an Euler integration is used to integrate Eq. (A1), this correction is equivalent to that developed by Inverarity (2000); cf. his Eqn. (12). However, this correction should be applied to the *recovery* temperature, not the *air* temperature. The sensor responds to the recovery temperature that includes the increase caused by dynamic heating, so applying the correction to the recovery temperature properly corrects for the response to dynamic heating also. Then the usual dynamic-heating correction can be subtracted to obtain an estimate of the air temperature.

The correction procedure must be modified for the heated sensor because, with the best-fit value $a = 0$, Eq. (6) can't be solved for $T_r(t)$. However, for $a = 0$ the differential equations can be combined to give

$$T_r(t) = (\tau_1 + \tau_2)\frac{dT_m(t)}{dt} + T_m(t) + \tau_2\tau_1\frac{d^2T_m(t)}{dt^2} \tag{A2}$$

This gives $T_r(t)$ without integration because finite-difference expressions can be used for the derivatives of the measurement ($T_m(t)$). However, the finite-difference estimates introduce high-frequency noise so the result was smoothed using a low-pass filter with 2 Hz cutoff frequency.

An alternate approach is to find the recovery temperature using Fourier transforms, from $T_r(t) = \mathrm{Re}\left(\mathcal{F}^{-1}\left(\hat{T}_m(\omega)/H(\omega)\right)\right)$ where Re denotes the real part of the complex result. Examples of the corrections produced by these two procedures are shown in Fig. A1. The agreement between the two correction methods is very good, and both show evidence of faster and higher-amplitude response to fluctuations. In comparison to the original measurement, the corrected values for the heated sensor are improved significantly by this correction procedure and are even a reasonable match to the corrected measurement from the faster unheated sensor.

If the response of the sensor is indeed linear, as the differential equations indicate, a correction procedure equivalent to that described above is first to filter the dynamic-heating term as in Sect. 3, correct the measured recovery temperature by

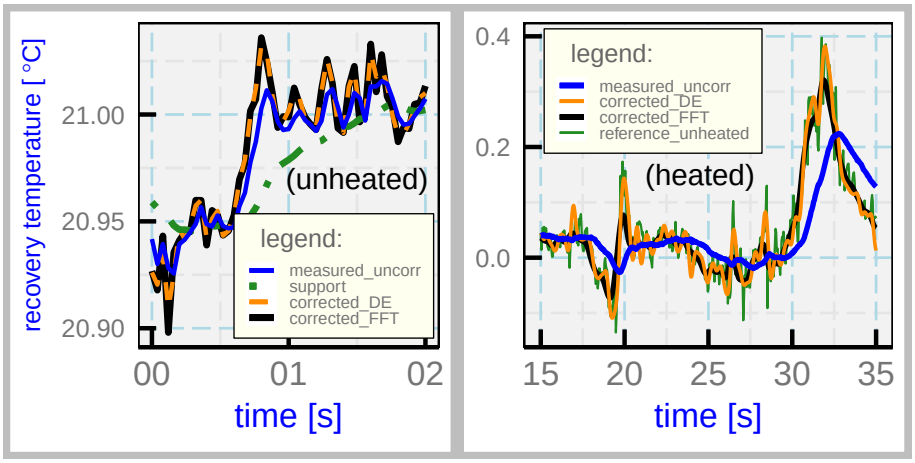

Figure A1. Examples of the corrected recovery temperatures compared to the original uncorrected measurements. In each case, the correction based on the differential equations is shown as "corrected_DE" and that based on Fourier transforms is labeled "corrected_FFT." The dashed green line in the left plot shows the calculated temperature of the support that contacts the sensing wire. The solid green line in the right plot shows the corrected measurement from the unheated sensor for comparison. (left): An unheated sensor. Measurements from VOCALS flight 3. (right): A heated sensor. In this case the "corrected_DE" result is based on Eq. (A2) while "corrected_FFT" uses the fit provided by Eq. (17). Mean values have been subtracted to facilitate comparison.

subtracting this filtered term, and then apply the correction procedure described above to the resulting air temperature to obtain the corrected air temperature.

Code and data availability. The data files used in this analysis are curated as indicated by the following references and are publicly available. They can be requested from the National Center for Atmospheric Research, Earth Observing Laboratory, at this web site: https://data.eol.ucar.edu. The files with references are as follows:

Research Project	Citation (see References)
VOCALS	UCAR/NCAR - Earth Observing Laboratory (2011)
CSET	UCAR/NCAR - Earth Observing Laboratory (2017)
SOCRATES	UCAR/NCAR - Earth Observing Laboratory (2019)

This document is constructed in ways that support duplication of the study. The code that generates the plots and implements the correction procedure is incorporated into the same file that generated this document via LaTeX, using principles and techniques described by Xie (2013) as implemented in the R package "knitr" (Xie, 2014). The program, "SensibleHeatFluxAMT.Rmd" is archived on "GitHub" in the directory at this URL. There is some supplemental material in that directory, including a workflow document and some code segments saved in the "chunks" subdirectory. The full directory should be downloaded in order to run the program. The calculations use the programming language R (R Core Team, 2019) and were run within RStudio (RStudio, 2009). A package named Ranadu (Cooper, 2020), containing auxillary functions, was used extensively in the R code and can be downloaded from that reference.

Author contributions. The first author wrote the processing code and developed the general idea for the paper. The second author contributed significantly to the manuscript and the presentation, and the third author provided Laplace-transform solutions and a digital filter based on them while also contributing to the presentation.

Competing interests. The authors declare no competing interests.

Acknowledgements. This material is based upon work supported by the National Center for Atmospheric Research, which is a major facility sponsored by the National Science Foundation under Cooperative Agreement No. 1852977. Data provided by NCAR/EOL under the sponsorship of the National Science Foundation. Measurements used here (UCAR/NCAR - Earth Observing Laboratory (2011), UCAR/NCAR - Earth Observing Laboratory (2019), UCAR/NCAR - Earth Observing Laboratory (2018)) were collected in research projects (Wood et al. (2011), Albrecht et al. (2019), McFarquhar et al. (2014)) that used the NSF/NCAR research aircraft. Project descriptions and additional The referenced project teams conducted the experiments, with flight operations, data acquisition and processing, and other project support by the Research Aviation Facility, Earth Observing Laboratory, National Center for Atmospheric Research (NCAR). The analyses reported here were mostly performed using R (R Core Team (2019)), with RStudio (RStudio (2009)) and knitr (Xie (2013, 2014)). Data files in netCDF format have been read and written using the R package "ncdf4" cf. Pierce (2015). Substantial use also was made of the "ggplot2" package (Wickham (2009)) for R, and extensive use was made of the "stats" package, part of Core R. Some of the numerical integrations used the Runge-Kutta function from the "rmutil" package (Swihart and Lindsey (2019)). The Copernicus template provided by Daniel Nüst, which uses the "rticles" package for R (Allaire et al. (2020)), was used with "RMarkdown" (Xie et al. (2018)) to generate this paper.

References

Albrecht, B. A., Ghate, V., Mohrmann, J., Wood, R., Zuidema, P., Bretherton, C. S., Schwartz, C., Eloranta, E., Glienke, S., Donaher, S., Sarkar, M., McGibbon, J., Nugent, A. D., Shaw, R. A., Fugal, J., Minnis, P., Paliknoda, R., Lussier, L., Jensen, J. B., Vivekanandan, J., Ellis, S., Tsai, P., Rilling, R., Haggerty, J., Campos, T., Stell, M., Reeves, M., Beaton, S., Allison, J., Stossmeister, G., Hall, S., and Schmidt, S.: Cloud System Evolution in the Trades (CSET): Following the Evolution of Boundary Layer Cloud Systems with the NSF–NCAR GV, Bulletin of the American Meteorological Society, 100, 93–121, https://doi.org/10.1175/BAMS-D-17-0180.1, https://doi.org/10.1175/BAMS-D-17-0180.1, 2019.

Allaire, J., Xie, Y., R Foundation, Wickham, H., Journal of Statistical Software, Vaidyanathan, R., Association for Computing Machinery, Boettiger, C., Elsevier, Broman, K., Mueller, K., Quast, B., Pruim, R., Marwick, B., Wickham, C., Keyes, O., Yu, M., Emaasit, D., Onkelinx, T., Gasparini, A., Desautels, M.-A., Leutnant, D., MDPI, Taylor and Francis, Öğreden, O., Hance, D., Nüst, D., Uvesten, P., Campitelli, E., Muschelli, J., Kamvar, Z. N., Ross, N., Cannoodt, R., Luguern, D., and Kaplan, D. M.: rticles: Article Formats for R Markdown, https://CRAN.R-project.org/package=rticles, r package version 0.14, 2020.

Bange, J., Esposito, M., Lenschow, D. H., Brown, P. R. A., Dreiling, V., Giez, A., Mahrt, L., Malinowski, S. P., Rodi, A. R., Shaw, R. A., Siebert, H., Smit, H., and Zöger, M.: Measurement of Aircraft State and Thermodynamic and Dynamic Variables, chap. 2, pp. 7–75, John Wiley & Sons, Ltd, https://doi.org/10.1002/9783527653218.ch2, https://onlinelibrary.wiley.com/doi/abs/10.1002/9783527653218.ch2, 2013.

Cash, J. R. and Karp, A. H.: A variable order Runge-Kutta method for initial value problems with rapidly varying right-hand sides, ACM Transactions on Mathematical Software (TOMS), 16, 201–222, 1990.

Cooper, W. A.: RANADU: R-Based Analysis for NCAR Aircraft Data Users (Version 2.6_20.05.15)., http://doi.org/10.5281/zenodo.3830427, 2020.

Cooper, W. A., Friesen, R. B., Hayman, M., Jensen, J. B., Lenschow, D. H., Romashkin, P. A., Schanot, A. J., Spuler, S. M., Stith, J. L., and Wolff, C.: Characterization of uncertainty in measurements of wind from the NSF/NCAR Gulfstream V research aircraft, NCAR technical note NCAR/TN-528+STR, Earth Observing Laboratory, NCAR, Boulder, CO, USA, http://n2t.net/ark:/85065/d7qr4zqr, 2016.

Foken, T., Wimmer, F., Mauder, M., Thomas, C., and Liebethal, C.: Some aspects of the energy balance closure problem, Atmospheric Chemistry and Physics, 6, 4395–4402, https://www.ingentaconnect.com/content/doaj/16807316/2006/00000006/00000012/art00021, 2006.

Foster, S. and Chan, P.: Improving the wind and temperature measurements of an airborne meteorological measuring system, Journal of Zhejiang University SCIENCE A, 13, 723–746, 2012.

Friehe, C. A. and Khelif, D.: Fast-response aircraft temperature sensors, J. Atmos. Ocean. Technol., 9, 784–795, https://doi.org/10.1175/1520-0426(1992)009<0784:FRATS>2.0.CO;2, 1992.

Hartmann, D. L.: Chapter 4 - The Energy Balance of the Surface, in: Global Physical Climatology (Second Edition), edited by Hartmann, D. L., pp. 95–130, Elsevier, Boston, second edition edn., https://doi.org/10.1016/B978-0-12-328531-7.00004-9, http://www.sciencedirect.com/science/article/pii/B9780123285317000049, 2016.

Inverarity, G. W.: Correcting Airborne Temperature Data for Lags Introduced by Instruments with Two-Time-Constant Responses, Journal of Atmospheric and Oceanic Technology, 17, 176–184, https://doi.org/10.1175/1520-0426(2000)017<0176:CATDFL>2.0.CO;2, https://doi.org/10.1175/1520-0426(2000)017<0176:CATDFL>2.0.CO;2, 2000.

Lawson, R. P. and Rodi, A. R.: A New Airborne Thermometer for Atmospheric and Cloud Physics Research. Part I: Design and Preliminary Flight Tests, Journal of Atmospheric and Oceanic Technology, 9, 556–574, https://doi.org/10.1175/1520-0426(1992)009<0556:ANATFA>2.0.CO;2, https://doi.org/10.1175/1520-0426(1992)009<0556:ANATFA>2.0.CO;2, 1992.

Lenschow, D., Mann, J., and Kristensen, L.: How long is long enough when measuring fluxes and other turbulence statistics?, Journal of Atmospheric and Oceanic Technology, 11, 661–673, 1994.

Lenschow, D. H.: The measurement of air velocity and temperature using the NCAR Buffalo Aircraft Measuring System, Tech. rep., https://doi.org/10.5065/D6C8277W, http://nldr.library.ucar.edu/repository/collections/TECH-NOTE-000-000-000-064, 1972.

Lenschow, D. H.: Micrometeorological techniques for measuring biosphere-atmosphere trace gas exchange, in: Biogenic trace gases: Measuring emissions from soil and water, edited by Matson, P. A. and Harriss, R. A., chap. 5, pp. 126–163, Blackwell Science Ltd., 1995.

Lenschow, D. H. and Stankov, B. B.: Length scales in the convective boundary layer, Journal of the Atmospheric Sciences, 43, 1198–1209, 1986.

McCarthy, J.: A method for correcting airborne temperature data for sensor response time, Journal of Applied Meteorology, 12, 211–214, 1973.

McFarquhar, G. M., Wood, R., Bretherton, C. S., Alexander, S., Jakob, C., Marchand, R., Protat, A., Quinn, P., Siems, S. T., and Weller, R. A.: The Southern Ocean Clouds, Radiation, Aerosol Transport Experimental Study (SOCRATES): An Observational Campaign for Determining Role of Clouds, Aerosols and Radiation in Climate System, in: AGU Fall Meeting Abstracts, 2014.

Nicholls, S.: Measurements of turbulence by an instrumented aircraft in a convective atmospheric boundary layer over the sea, Quarterly Journal of the Royal Meteorological Society, 104, 653–676, 1978.

Payne, G. A., Friehe, C. A., and Edwards, D. K.: Time and Frequency Response of a Resistance-Wire Aircraft Atmospheric Temperature Sensor, Journal of Atmospheric and Oceanic Technology, 11, 463–475, https://doi.org/10.1175/1520-0426(1994)011<0463:TAFROA>2.0.CO;2, https://doi.org/10.1175/1520-0426(1994)011<0463:TAFROA>2.0.CO;2, 1994.

Pierce, D.: ncdf4: Interface to Unidata netCDF (Version 4 or Earlier) Format Data Files, https://CRAN.R-project.org/package=ncdf4, r package version 1.15, 2015.

R Core Team: R: A language and environment for statistical computing, R Foundation for Statistical Computing, Vienna, Austria, http://www.R-project.org, 2019.

Rodi, A. R. and Spyers-Duran, P. A.: Analysis of time response of airborne temperature sensors, Journal of Applied Meteorology, 11, 554–556, 1972.

RStudio: RStudio: Integrated development environment for R (Version 0.98.879), http://www.rstudio.org, 2009.

Stickney, T. M., Shedlov, M. W., and Thompson, D. I.: Goodrich total temperature sensors, Goodrich Technical Report 5755 Revision C, Rosemount Aerospace Inc., http://www.faam.ac.uk/index.php/component/docman/doc_download/47-rosemount-report-5755(lastaccess: 8Aug2014), 1994.

Swihart, B. and Lindsey, J.: rmutil: Utilities for Nonlinear Regression and Repeated Measurements Models, https://CRAN.R-project.org/package=rmutil, r package version 1.1.3, 2019.

UCAR/NCAR - Earth Observing Laboratory: NCAR/NSF C-130 Navigation, State Parameter, and Microphysics HRT (25 sps) Data. Version 1.0 [Data set, VOCALS], https://doi.org/10.5065/d69k48jk, https://doi.org/10.5065/d69k48jk,Accessed09Jan2020, 2011.

UCAR/NCAR - Earth Observing Laboratory: High Rate (HRT - 25 sps) Navigation, State Parameter, and Microphysics Flight-Level Data. Version 2.0. [Data set, CSET], https://doi.org/10.5065/D63R0R3W, https://doi.org/10.5065/D63R0R3W,Accessed12Mar2020, 2017.

UCAR/NCAR - Earth Observing Laboratory: High Rate (HRT - 25 sps) Navigation, State Parameter, and Microphysics Flight-Level Data. Version 0.1 [PRELIMINARY] [Data set, WE-CAN], https://data.eol.ucar.edu/dataset/548.004.Accessed09Jan2020., 2018.

UCAR/NCAR - Earth Observing Laboratory: High Rate (HRT) Navigation, State Parameter, and Microphysics Flight Level Data. Version 1.0 [Data set, SOCRATES], https://doi.org/10.26023/K5VQ-K6KY-W610, https://doi.org/10.26023/K5VQ-K6KY-W610, Accessed09Jan2020, 2019.

Wickham, H.: ggplot2: elegant graphics for data analysis, Springer New York, http://had.co.nz/ggplot2/book, 2009.

Wood, R., Mechoso, C. R., Bretherton, C. S., Weller, R. A., Huebert, B. J., Straneo, F., Albrecht, B. A., Coe, H., Allen, G., Vaughan, G., et al.: The VAMOS Ocean-Cloud-Atmosphere-Land Study Regional Experiment (VOCALS-REx): goals, platforms, and field operations., 2011.

Xie, Y.: Dynamic Documents with R and knitr, Chapman and Hall/CRC, Boca Raton, Florida, http://yihui.name/knitr/, iSBN 978-1482203530, 2013.

Xie, Y.: knitr: A general-purpose package for dynamic report generation in R, http://yihui.name/knitr/, r package version 1.6, 2014.

Xie, Y., Allaire, J., and Grolemund, G.: R Markdown: The Definitive Guide, Chapman and Hall/CRC, Boca Raton, Florida, https://bookdown.org/yihui/rmarkdown, iSBN 9781138359338, 2018.